Archimedean-like colloidal tilings on substrates with decagonal and tetradecagonal symmetry

Michael Schmiedeberg[1], Jules Mikhael[2], Sebastian Rausch[2], Johannes Roth[3], Laurent Helden[2], Clemens Bechinger[2,4], and Holger Stark[5]

[1] Department of Physics and Astronomy, University of Pennsylvania, 209 South 33rd Street, Philadelphia, PA 19104, USA
[2] 2. Physikalisches Institut, Universität Stuttgart, Pfaffenwaldring 57, D-70550 Stuttgart, Germany
[3] Institut für Theoretische und Angewandte Physik, Universität Stuttgart, Pfaffenwaldring 57, D-70550 Stuttgart, Germany
[4] Max-Planck-Institut für Metallforschung, Heisenbergstraße 3, D-70569 Stuttgart, Germany
[5] Institut für Theoretische Physik, Technische Universität Berlin, Hardenbergstr. 36, D-10623 Berlin, Germany

Abstract. Two-dimensional colloidal suspensions subject to laser interference patterns with decagonal symmetry can form an Archimedean-like tiling phase where rows of squares and triangles order aperiodically along one direction [J. Mikhael *et al.*, Nature **454**, 501 (2008)]. In experiments as well as in Monte-Carlo and Brownian dynamics simulations, we identify a similar phase when the laser field possesses tetradecagonal symmetry We characterize the structure of both Archimedean-like tilings in detail and point out how the tilings differ from each other. Furthermore, we also estimate specific particle densities where the Archimedean-like tiling phases occur. Finally, using Brownian dynamics simulations we demonstrate how phasonic distortions of the decagonal laser field influence the Archimedean-like tiling. In particular, the domain size of the tiling can be enlarged by phasonic drifts and constant gradients in the phasonic displacement. We demonstrate that the latter occurs when the interfering laser beams are not adjusted properly.

PACS. 61.44.Br Quasicrystals – 82.70.Dd Colloids

1 Introduction

Unlike ordinary crystals, quasicrystals possess point-symmetries, e.g., with five- or ten-fold rotational axes, which are not allowed in periodic crystals [1,2]. Nevertheless, quasicrystals exhibit Bragg-reflections due to their long-range positional and orientational order. Since they show exceptional material properties [3], there is much interest in understanding and controlling the growth of quasicrystals. Therefore, a lot of research has been devoted to study the ordering of atoms on quasicrystalline surfaces [4,5,6, 7,8,9,10,11,12,13,14,15]. However, in these experiments it is very difficult to determine the exact positions of the atoms. Therefore, a model system consisting of micronsized colloidal particles subject to a laser interference pattern has been used to investigate the dynamics and ordering of particles in a two-dimensional quasicrystalline potential [16,17,18,19,20]. Interesting structures have been observed, such as phases with 20 bond directions [19] or colloidal orderings consisting of rows of squares and rows of triangles termed Archimedean-like tilings [18,19] (see also Fig. 1). The latter will be the main topic of this work.

Interference patterns of five or seven laser beams have decagonal or tetradecagonal symmetry, respectively (see Fig. 2). In such laser fields, the colloids are forced towards the regions with highest laser intensity, i.e., for the
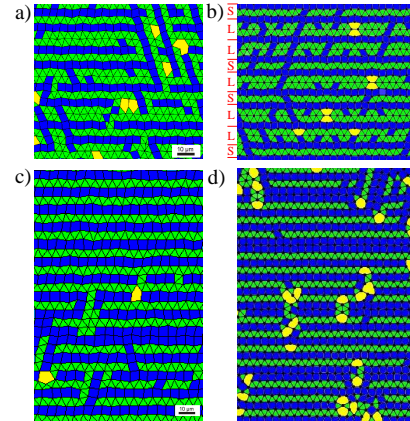

Fig. 1. Archimedean-like tiling phases induced by (a,b) the decagonal and (c,d) the tetradecagonal substrate. (a,c) show experimental results, (b,d) are obtained by Monte-Carlo simulations. The figures show Delaunay triangulations of colloidal point patterns. Bonds longer than $1.1a_S$ ($1.2a_S$ for experiments) are omitted, where a_S is the spacing of the particles when placed on an ideal triangular lattice. The potential strength is $V_0/(k_B T) = 13$ in (a), $V_0/(k_B T) = 10$ in (c), and $V_0/(k_B T) = 20$ in the simulations (b,d). The density is given by $a_S/a_V = 0.57$ in (a), $a_S/a_V = 0.58$ in (b), and $a_S/a_V = 0.7$ in (c,d).
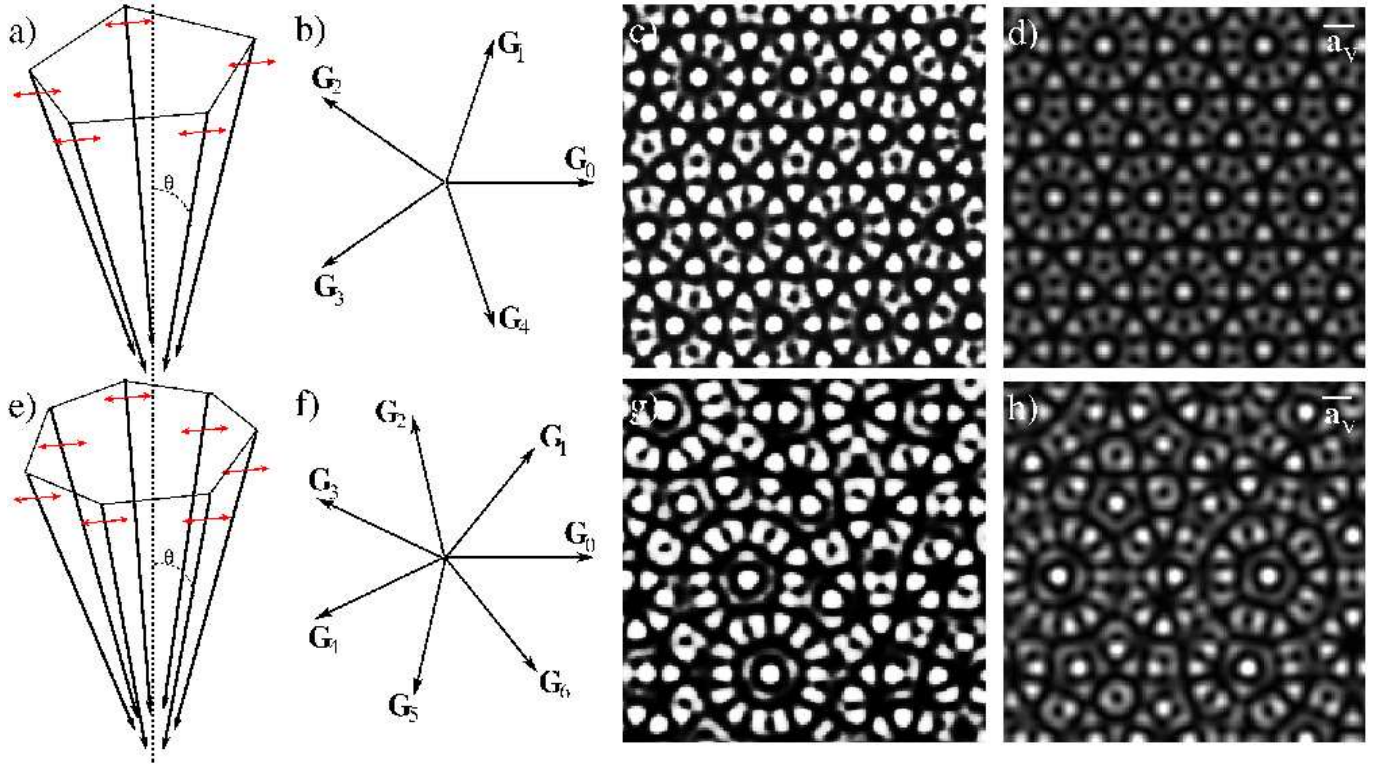
Fig. 2. The external potentials are created by interfering laser beams with a symmetric arrangement. An interference pattern with 10-fold rotational symmetry is obtained with five laser beams (a-d), 14-fold symmetry is realized with seven beams (e-h). (a,e) show how the laser beams are arranged and (b,f) the wave-vectors projected onto the sample plane. (c,g) demonstrate the interference patterns observed in experiments, and in (d,h) they are calculated from Eq. (1). The bar in the upper right corners of (d,h) denote the length scale $a_V = 2\pi/|\mathbf{G}_j|$, where $\mathbf{G}_j$ are the projected wave vectors as shown in (b,f).

colloidal particles the interference patterns act like a substrate with quasicrystalline symmetry. If the influence of the laser field is weak, the colloidal particles form a triangular lattice in case of sufficiently strong repulsion forces or they are in a fluid phase when colloidal interactions are weak. For large laser intensities, the ordering of the colloids is determined by the interference pattern, i.e., a quasicrystalline phase is observed (see also the phase diagrams in Fig. 3 and in [19]). In this work we are especially interested in phases that occur at intermediate laser strengths where there is a competition between the repulsive colloidal interactions (that alone would lead to periodic triangular ordering) and the external forces due to the laser field which favor aperiodic quasicrystalline structures. For certain particle densities that we will determine later in this article, the competition leads to a colloidal ordering that consists of rows of triangles and rows of squares that establish an aperiodic order in one spatial direction. (see Fig. 1). The structure observed is close to an Archimedean tiling, where the rows of squares and triangles form a two-dimensional periodic order. It was therefore named Archimedean-like tiling when it was first realized in experiments using laser fields with decagonal symmetry [18]. Later Archimedean-like tilings also occured in simulations that studied the complete phase behavior on a decagonal substrate ([19], see also Fig. 3).

The purpose of this article is to characterize the structure of the Archimedean-like tiling phases in detail, to discuss the differences of the ordering in laser fields with decagonal and tetradecagonal symmetry, and finally to determine the densities where these phases occur. In addition, we study the influence of phasonic distortions on colloidal ordering in laser fields with decagonal symmetry. Phasons are excitations that only exist in quasicrystals. Like phonons, they are hydrodynamic modes, i.e., they do not cost free energy in the long-wave-length limit [21,22]. Phasons are an ongoing main topic in current research on quasicrystals and intensively discussed in the field [23,24,25].

In Sec. 2 we introduce our system. The details of the experimental realization as well as the numerical simulations are explained in Sec. 3. In Sec. 4 we analyze the structure of the Archimedean-like tilings and calculate the densities where these phases occur. We study the consequences of phasonic distortions on the Archimedean-like tilings in Sec. 5 and finally conclude in Sec. 6.

2 Model

A charged stabilized suspension is confined between two glass plates and subjected to laser interference patterns
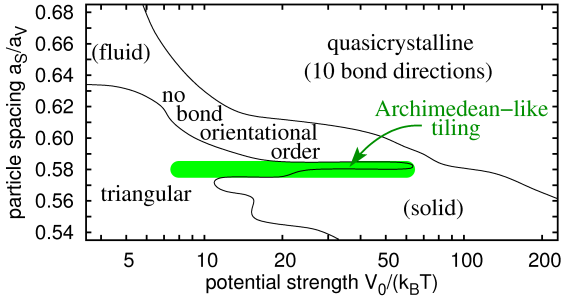
Fig. 3. Phase diagram obtained with Monte-Carlo simulations for colloids on the decagonal substrate (the complete phase diagrams are presented and explained in [19]). Unlike quasicrystalline phases that we observed at all densities, Archimedean-like tiling structures are only found for intermediate potential strengths within a small range of densities (marked green).

with quasicrystalline symmetries. Five or seven laser beams with identical linear polarizations are employed to obtain interference patterns with decagonal or tetradecagonal rotational symmetry, respectively (see Fig. 2). For vanishing tilt angle $\theta \to 0$ of the beams, the potential in the xy plane is [17,26]:

$$V(\mathbf{r}) = -\frac{V_0}{N^2} \sum_{j=0}^{N-1} \sum_{k=0}^{N-1} \cos\left[(\mathbf{G}_j - \mathbf{G}_k) \cdot \mathbf{r} + \phi_j - \phi_k\right], \quad (1)$$

where N is the number of beams, ϕ_j are the phases of the laser-light waves, and $\mathbf{G}_j$ their wave-vectors projected onto the xy plane [cf. Fig. 2(b) and (f)]. The prefactor is chosen such that $-V_0$ gives the minimum value of the potential. We usually set $\phi_j = 0$ for all j corresponding to a laser field without any phononic or phasonic displacements and a center of exact 10- or 14-fold rotational symmetry at $\mathbf{r} = \mathbf{0}$. In addition, for the decagonal potential, we explicitly analyze the effect of phasonic distortions on the Archimedean-like tiling in the last section. In this case, the phases ϕ_j are used to specify the phononic displacement field $\mathbf{u}(\mathbf{r},t) = [u_x(\mathbf{r},t), u_y(\mathbf{r},t)]$ and the phasonic field $\mathbf{w}(\mathbf{r},t) = [w_x(\mathbf{r},t), w_y(\mathbf{r},t)]$ following the convention of Ref. [21,22],

$$\phi_j(\mathbf{r},t) = \mathbf{u}(\mathbf{r},t) \cdot \mathbf{G}_j + \mathbf{w}(\mathbf{r},t) \cdot \mathbf{G}_{3j \bmod 5}. \quad (2)$$

In section 5 we will show how a uniform phasonic displacement $\mathbf{w}(\mathbf{r},t)$, which increases linearly in time, or how a static $\mathbf{w}(\mathbf{r},t)$ with a constant gradient can be used to align the rows of the Archimedean-like tiling phases along specific directions of the underlying substrate potential.

3 Methods

In the following, we shortly introduce our methods, which we employed to analyze the results from experiments and simulations.

3.1 Experiment

The colloidal system we used is an aqueous suspension of highly charged sulphate-terminated polystyrene particles with a radius of $R = 1.45$ μm from Interfacial Dynamics Corporation with an average polydispersity below 4%. The pair interaction of particles can be described by a screened Coulomb potential as introduced below in Eq. (3). As sample cell we used a silica glass cuvette with 200 μm spacing. Before starting the measurement, it was connected to a deionization circuit to reduce the salt concentration of the suspension. This circuit also included an electrical conductivity probe (typical ionic conductivities below 0.08 μS/cm), a vessel of ion exchange resin, and a peristaltic pump. After deionization, the suspension was inserted into the cell which was then sealed. Before applying the quasiperiodic potential, the density of the particles was increased in the field of view. This is achieved through thermophoretic and optical forces using vertically incident fiber coupled infrared laser with a wavelength of $\lambda = 1070$ nm and maximum output power $P_{\max} = 5$ W and an argon ion laser ($\lambda = 514$ nm, $P_{\max} = 7$ W). A circular monolayer was formed on the lower surface of the sample cell with a diameter of about 500 μm. The vertical fluctuations of the particles are also suppressed by the argon ion beam, therefore the system can be considered as two-dimensional. The monolayer spontaneously adapts the hexagonal packing. After reaching the desired particle density, the infrared laser was turned off. The high particle density was kept constant using an optical tweezer ($\lambda = 488$ nm, $P_{\max} = 7$ W) scanned around the central region of the system, i.e., forming a circular corral. The quasiperiodic potential was created by interference of five or seven linearly polarized beams of a Nd:YVO4 laser ($\lambda = 532$ nm, $P_{\max} = 18$ W). Due to optical gradient forces, this interference pattern acts as an external potential on the particles. The depth V_0 of the singular deepest potential well (see Sec. 2) scales linearly with the laser power. V_0 was determined by calibrating the laser intensity for three laser beams, i.e., when they create a triangular potential. The length scale a_V was tuned by changing the angle of incidence of the laser beams with respect to the sample plane. The different colloidal phases were identified with the help of a Delaunay triangulation. It creates nearest-neighbor bonds between vertices that were defined by the maxima of the colloidal density distribution. For Archimedean-like tiling structures the bond length is a bimodal distribution with the ratio of the peak positions close to $\sqrt{2}$. Bonds longer than $1.2a_S$ were removed from the triangulation which resulted in the characteristic square-triangle tiling.

3.2 Simulations

The interaction between the colloids is modeled by the pair potential

$$\phi(d) = \frac{[Z^* e \exp(\kappa R)]^2}{4\pi\epsilon_0 \epsilon_r (1 + \kappa R)^2} \frac{\exp(-\kappa d)}{d} \quad (3)$$

of the Derjaguin-Landau-Verwey-Overbeek theory [27,28], where d is the distance between two colloids and κ the inverse Debye screening length. The prefactor also depends on the radius R of a colloid, its effective surface charge Z^*, and the dielectric constant of water ϵ_r.

We quantify the particle density by the spacing a_S of the particles when placed on an ideal triangular lattice. The occurrence of Archimedean-like tilings mainly depends on the density of the system. All other parameters can be varied over huge ranges. The main limitation to the choice of parameters is that there has to be a competition between the colloidal interactions and the interaction with the substrate. Therefore, we usually choose the parameters such that the density used in the simulations is slightly above the density where the triangular to liquid phase transition occurs. For example, the parameter set for the decagonal substrate employed already in [19] is suitable to observe Archimedean-like tilings, i.e., $R = 1.2$ μm, $Z^* = 1000$, $\epsilon_r = 78$, $T = 300$ K, $a_V = 5.0$ μm, and $\kappa^{-1} = 0.25$ μm. Whereas a parameter set closer to the experimental values $R = 1.45$ μm, $Z^* = 400000$, $\epsilon_r = 78$, $T = 300$ K, $a_V = 6.5$ μm, and $\kappa^{-1} = 0.2$ μm (cf. [20]) was employed to simulate colloidal ordering in the tetradecagonal laser field. We usually performed Monte-Carlo simulations using the Metropolis algorithm [30]. Periodic boundary conditions were implemented for simulation boxes that contained about 500 to 1400 colloids. For comparison or to study dynamical properties, we also employed Brownian dynamics simulations as specified in [17].

When domains with Archimedean-like tiling structures occur, their rows are aligned along the respective five or seven equivalent directions of the laser potential. Usually within one simulation box, one finds many domains with different orientations. There is a tendency that small domains anneal out in time, i.e., adjacent domains grow slowly within the simulation process. The structures shown in Fig. 1 are about the largest domains we achieved by pure Monte-Carlo simulations. However, we discovered different methods to support the formation of larger domains. While in Monte-Carlo simulations the direction of a domain may change quite easily, such domain flips are rare in Brownian dynamics simulations. Therefore, Brownian dynamics simulations can help to grow large uniform domains. It is also possible to predefine a preferred direction. For example, by using small simulation boxes where the potential is discontinuous at the boundaries, the rows of an Archimedean-like tiling start to form along the boundaries. Furthermore, phasonic distortions support the growth of Archimedean-like tilings along specific directions as discussed in Sec. 5.

4 Archimedean-like tilings

The structures we observe in the two-dimensional quasicrystalline potentials at certain particle densities consist of rows of squares and rows of triangles and therefore are similar to the Archimedean tiling shown in Figure 4. In general, Archimedean tilings are formed by regular polygons and are characterized by the number of edges of the
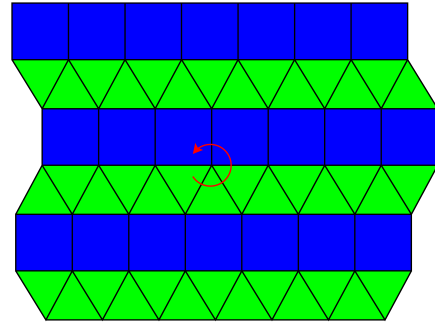

Fig. 4. Archimedean tiling of type $(3^3 \cdot 4^2)$.

polygons that meet in each vertex [31]. The tiling shown in Figure 4 is called $(3^3 \cdot 4^2)$-Archimedean tiling, because going around a vertex, one first finds three regular triangles and then two squares (see red arrow in Fig. 4). Very recently similar Archimedean tilings were also observed for binary mixtures of nanoparticles situated between a cubic and a dodecagonal phase [32]. Furthermore, an Archimedean tiling of type $(3^2 \cdot 4 \cdot 3 \cdot 4)$ occured in simulations of monoatomic systems on periodic substrates [33, 34,35,36].

4.1 On decagonal substrates

The Archimedean-like tiling on a decagonal substrate differs from the perfect $(3^3 \cdot 4^2)$-Archimedean tiling by the frequent appearance of double rows of triangles [see Figs. 1(a,b)]. From the simulation data we were able to identify the sequence over a range of $-6a_V \leq y \leq 100a_V$ that correspond to 77 single or double rows of triangles. Within this range the observed sequence is exactly the sequence of the Fibonacci chain, if one identifies a double row with L and a single row with S [cf. Fig. 1(b)]. A Fibonacci chain is obtained by starting with element L and repeatedly applying the iteration rules $L \rightarrow LS$ and $S \rightarrow L$. For example, the first iterations are L, LS, LSL, $LSLLS$, $LSLLSLSL$, etc..

Note, the squares and triangles of the Archimedean-like tiling are not perfect regular polygons. A row of triangles has almost the same height as a row of squares. In the simulations, we find the ratio of the mean row height l_y divided by the mean particle spacing l_x in the direction along the rows to be $l_y/l_x \approx 0.95$, i.e., the triangles are stretched in the direction perpendicular to the rows while the squares are stretched in the direction along the rows. We will calculate the ratio l_y/l_x in subsection 4.3.

At a first glance, the Archimedean-like tiling structure seems to be periodic along the rows of triangles. However, some aperiodic modulations along the rows can be observed. For example, in the structures shown in Figs. 1(a,b) only very few bonds are perfectly horizontal. Whereas most of the bonds between two neighboring rows of triangles are almost horizontal, the direction of all other bonds deviate from the horizontal direction in an aperiodic way. Furthermore, there is a modulation of the bond lengths
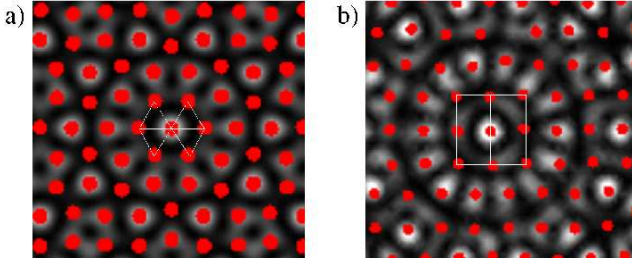
Fig. 5. Colloidal order close to symmetry centers in simulations: (a) On decagonal substrates double rows of triangles occur at symmetry centers, (b) in tetradecagonal laser fields double rows of squares are found.

along the direction of the rows. As a result, some rows of squares exist along a direction that is rotated by $2\pi/5$ from the main horizontal row direction.

4.2 On tetradecagonal substrates

The Archimedean-like tiling phase on a tetradecagonal substrate consists of large periodic regions that correspond to a perfect Archimedean tiling of type $(3^3 \cdot 4^2)$. The periodicity is only interrupted by a few double rows of squares. Fig. 5(b) shows the position of the colloids on the substrate. Obviously, a double row of squares occurs at a local symmetry center of the laser field. This bright spot corresponds to a deep potential minimum that is surrounded by 14 shallower potential wells. It therefore constitutes the center of a region with 14-fold rotational symmetry. Since in a tetradecagonal laser field local symmetry centers are rare [20], only few double rows of squares exist in the Archimedean-like tiling structure. Fig. 5(a) demonstrates that for the decagonal substrate double rows of triangles occur at symmetry centers. Since there are much more symmetry centers in a decagonal laser field [20], much more double rows exist in the Archimedean-like tiling phase of a decagonal substrate compared to a tetradecagonal laser field.

4.3 Densities with Archimedean-like tilings

In the following, we want to estimate the densities where Archimedean-like tiling structures occur. At a suitable density, the rows of colloids should be oriented along lines with many minima of the potential landscape. In the decagonal laser field, we can determine the distances between such lines by averaging the potential $V(\mathbf{r})$ along the x-direction, i.e.,

$$\langle V \rangle_x = \frac{V_0}{25} \left[-5 - 2\cos\left(2\pi y/\lambda_1\right) - 2\cos\left(2\pi y/\lambda_2\right) \right], \quad (4)$$

$$\text{with} \quad \lambda_1 = \sqrt{\frac{5 - \sqrt{5}}{10}} \, a_V$$

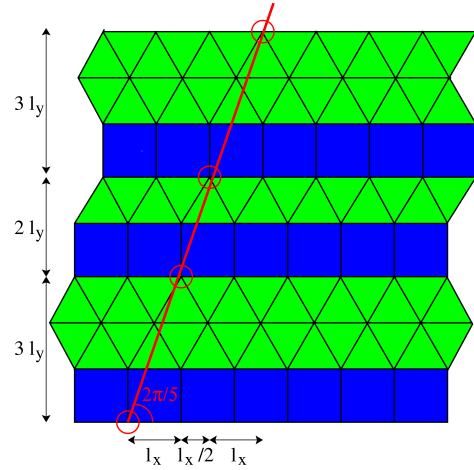$$\text{and} \quad \lambda_2 = \sqrt{\frac{5 + \sqrt{5}}{10}} \, a_V.$$

Fig. 6. We calculate the mean bond length in horizontal direction l_x in a way that many colloids lie along the $2\pi/5$-direction (circled red). The mean row hight l_y is chosen to fit one of the two length scales of the substrate in y-direction.

We now calculate the density of an Archimedean-like tiling whose mean row height l_y fits to one of the lengths λ_1 or λ_2.

The simulation results show that the mean bond length l_x in the direction of the rows differs from the row height l_y. Therefore, in the following, we aim at calculating the ratio l_y/l_x. So far we have determined the row height l_y of an Archimedean-like tiling that fits to the decagonal substrate. To estimate the bond length l_x, we argue as follows. The rows are oriented along a symmetry direction of the decagonal potential. On this direction many potential minima are situated that are occupied by the particles. However, an equivalent symmetry direction is found at an angle of $2\pi/5$ with the rows. It should also be occupied by as much particles as possible. Figure 6 demonstrates how this direction can be fitted to the Archimedean-like tiling. Colloids close to the red line are marked by red circles. In case of a single row of triangles, to move from one particle to another close to the red line, one steps $l_x/2$ in x-direction and $2l_y$ in y-direction. In case of a double row of triangles, the step lenghts are l_x in x-direction and $3l_y$ in y-direction. The sequence of single and double rows corresponds to the sequence of the Fibonacci chain. Therefore, there are τ times as many double rows as single rows of triangles, where $\tau = \left(1 + \sqrt{5}\right)/2 \approx 1.618$ is the number of the golden mean. As a consequence, the orientation of the red line is determined by

$$\tan\left(2\pi/5\right) = \frac{(2 + 3\tau)\, l_y}{\left(\frac{1}{2} + \tau\right) l_x}, \quad (5)$$

i.e., we find the ratio $l_y/l_x \approx 0.951$ which agrees remarkably well with the value determined from simulations in subsection 4.1.

To calculate the mean particle spacing a_S, we compare the number density in the Archimedean-like tiling,
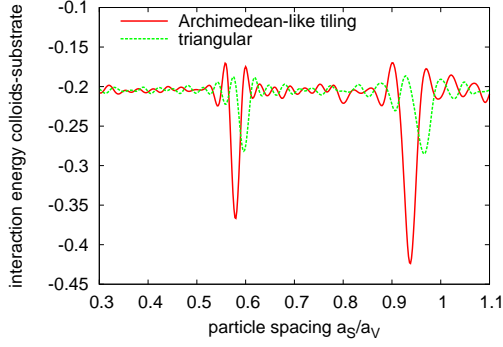
$$\rho = \frac{1}{l_x l_y} \,, \quad (6)$$

Fig. 7. Average potential energy of a colloid in the decagonal potential calculated for a triangular and for an Archimedean-like tiling structure as a function of density, which is given by the particle spacing a_S/a_V. To determine the average potential energy, we constructed a perfect triangular or Archimedean-like tiling structure with the corresponding particle spacing and calculated the average potential depth at the positions of the colloids of the structure.

with the number density of a triangular lattice $\rho = 2/\left(\sqrt{3}a_S^2\right)$. By using l_x from Eq. (5), we find for the mean particle spacing of the Archimedean-like tiling,

$$a_S = \sqrt{\frac{2}{\sqrt{3}}\frac{2+3\tau}{\frac{1}{2}+\tau}\frac{1}{\tan\left(2\pi/5\right)}}\, l_y = \left[\frac{8}{15}\left(5-\sqrt{5}\right)\right]^{\frac{1}{4}} l_y,$$
(7)

where l_y has to be one of the length scales $\lambda_{1,2}$ introduced in Eq. (4). Therefore, Archimedean-like tilings on the decagonal substrate occur for

$$a_S/a_V = 2\left[\frac{1}{75}\left(5-2\sqrt{5}\right)\right]^{\frac{1}{4}} \approx 0.579$$

$$\text{or } a_S/a_V = \left[\frac{8}{75}\left(5+\sqrt{5}\right)\right]^{\frac{1}{4}} \approx 0.937.$$
(8)

Indeed, in experiments and in simulations, we find the Archimedean-like tiling structures for densities close to these theoretical values (see, e.g., phase diagram in Fig. 3).

In Fig. 7 we show how the average potential energy of a colloid varies with density when it is part of either a triangular lattice or an Archimedean-like tiling structure under the influence of the decagonal substrate potential. We assumed that the Archimedean-like tiling structure is stretched perpendicular to the direction of the rows such that Eq. (5) holds. From Fig. 7 we can clearly identify two densities where the Archimedean-like tiling fits to the substrate very well. Most of the colloids are located in minima of the potential and therefore the average potential energy exhibits two sharp minima. These densities correspond to the values calculated in Eq. (8). Note, we also determined the average potential energy for other Archimedean tilings, but did not find any other structure that shows pronounced minima. For example, an Archimedean tiling
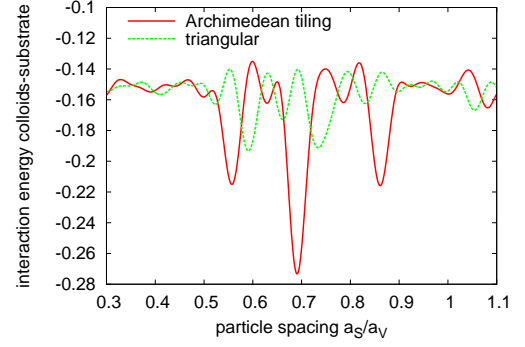
Fig. 8. Average potential energy of a colloid in the tetradecagonal potential calculated for a triangular and for an Archimedean-like tiling structure as a function of density, which is given by the particle spacing a_S/a_V.
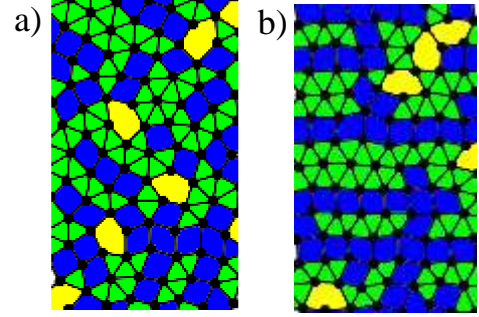

Fig. 9. Brownian dynamics simulation without confining boundaries started at an initial density that corresponds to $a_S/a_V = 0.565$. (a) Delaunay construction (as in Fig. 1) displaying the colloidal configuration when the simulation starts ($t = 0$). After time $t = 0.05\gamma a_V^2/k_B T$, where γ is the friction coefficient of a colloid, an Archimedean-like tiling structure can be observed which remains almost unchanged up to the end of our simulation at time $t = 0.25\gamma a_V^2/k_B T$ shown in (b). Note, while the Archimedean-like tilings shown in Fig. 1 are equilibrium phases that occur in systems with densities fixed at special values, the structure in (b) is only metastable because it will slowly dissolve when the density decreases due to the missing boundaries.

of type $(3^2 \cdot 4 \cdot 3 \cdot 4)$ has exactly the same particle interaction energy as the tiling of type $(3^3 \cdot 4^2)$. However, by comparing the average potential energies, we find that the substrate favors the row structure corresponding to type $(3^3 \cdot 4^2)$.

To determine the densities, where Archimedean-like tilings occur under the influence of the tetradecagonal substrate potential, we calculate the average potential energy of a colloid within an Archimedean tiling structure as a function of the particle spacing (see Fig. 8). Again, we find pronounced minima of the potential energy (although not as sharp as for decagonal potentials) at $a_S/a_V = 0.557$, $a_S/a_V = 0.691$, and $a_S/a_V = 0.861$. At these values we were indeed able to observe Archimedean-like tilings in the simulations.

We just argued that Archimedean-like tilings should only occur at specific densities. Correspondingly, when using Monte-Carlo simulations to find the equilibrium phases, we only observe them close to the calculated densities, e.g., in a narrow density region in the phase diagram of Fig. 3. Whereas in the simulations the density is a constant quantity, it can to a certain degree change its value in experiments; the experimental system is large enough that the density can become non-uniform and colloids can leave the boundary box. Indeed, when in the experiment we bring the density close to the ones predicted by Eq. (8), we observe that the colloids self-adjust their density so that the Archimedean-like tiling forms. Figure 7 explains this observation since the energy is lowered by forming an Archimedean-like tiling, at least relative to the triangular phase. To further investigate the idea of self-adjusting the colloidal density, we performed the following Brownian dynamics simulations: We confine the colloids at a density given by $a_S/a_V = 0.565$ that is larger than the one suitable for Archimedean-like tilings ($a_S/a_V = 0.58$). We then remove the confining boundaries so that the colloids are able to float over the substrate potential and the system expands. Indeed, we find that particles adjust to the potential by forming the characteristic rows of squares and triangles of an Archimedean-like tiling (see Fig. 9). Of course, this structure is not the thermodynamic ground state in such an open system. However, it remains present during the duration of the simulation which is the time a free particle would need to diffuse a distance a_V. Only at the edges of an Archimedean-like tiling domain does the structure start to dissolve. This demonstrates while Archimedean-like tilings are equilibrium phases at special densities only, they also occur as metastable structures in systems with open boundaries.

5 Phasonic Distortions

In this section we demonstrate, how the ordering of colloids in the Archimedean-like tiling that forms in the decagonal laser field is affected by manipulating the phasonic degrees of freedom as defined in Eq. (2). The consequences of a constant phasonic displacement on a quasicrystalline phase with decagonal symmetry were presented in [19].

5.1 Inducing Phasonic Flips

We first study how a constant phasonic displacement influences the Archimedean-like tiling. Figure 10 shows patterns of the Archimedean-like tiling in the decagonal laser field for different phasonic components $w_y = 0$ and $w_y = 0.015a_V$. Note, a whole row of triangles and a row of squares have interchanged their position. This corresponds to a phasonic flip in the Fibonacci chain defined by the sequence of long and short distances between the square rows.

Figure 2 (d) shows very clearly sets of parallel lines of low intensity in the decagonal laser field that are oriented
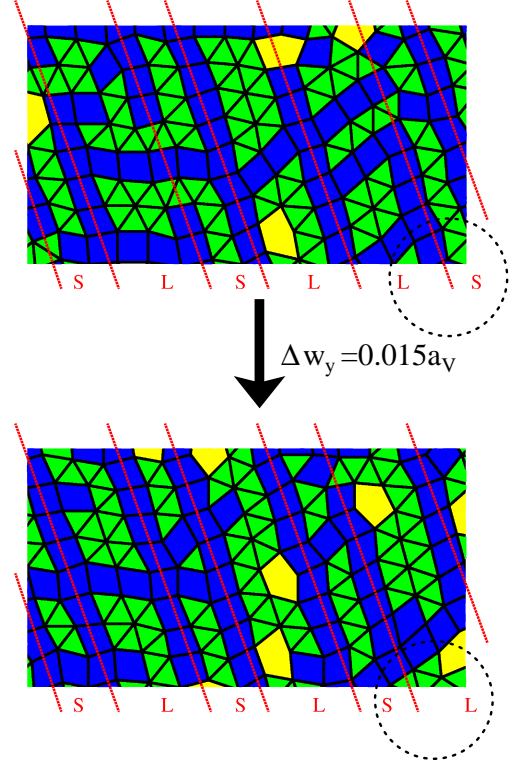

Fig. 10. Inducing a phasonic flip: Delaunay construction (as in Fig. 1) for the Archimedean-like tiling phase ($a_S/a_V = 0.577$, $V_0/(k_B T) = 20$) obtained by Monte-Carlo simulations for $w_y = 0$ (top) and $w_y = 0.015a_V$ (bottom). The flip in the Fibonacci chain defined by the single and double rows of triangles is marked by dotted circles.

along its five equivalent directions. One can choose phasonic displacements such that one set of dark parallel lines does not change. So if the square and triangular rows are parallel to this set of lines, the whole Archimedean-like tiling is not affected by the phasonic displacement. For example, a phasonic displacement w_x does not influence the square and triangular rows when they are oriented along the x direction. As we show in the next subsection, a phasonic drift in w_x may even help to stabilize the Archimedean-like tiling structure.

5.2 Stabilization by Phasonic Drifts and Gradients

A steadily growing w_x in time orients the Archimedean-like tiling along the x-direction. This is demonstrated in Fig. 11 for a phasonic drift velocity $\Delta w_x = 10^{-4} a_V$ per unit time. Domains that are not oriented along the x-direction are reduced since a nonzero Δw_x constantly induces phasonic flips in the rows of squares and triangles of the Archimedean-like tiling unless they are oriented along the x-direction. Another way of explaining the consequences of the phasonic drift velocity Δw_x goes as follows. One can demonstrate that a steadily growing phasonic displacement rearranges the decagonal potential

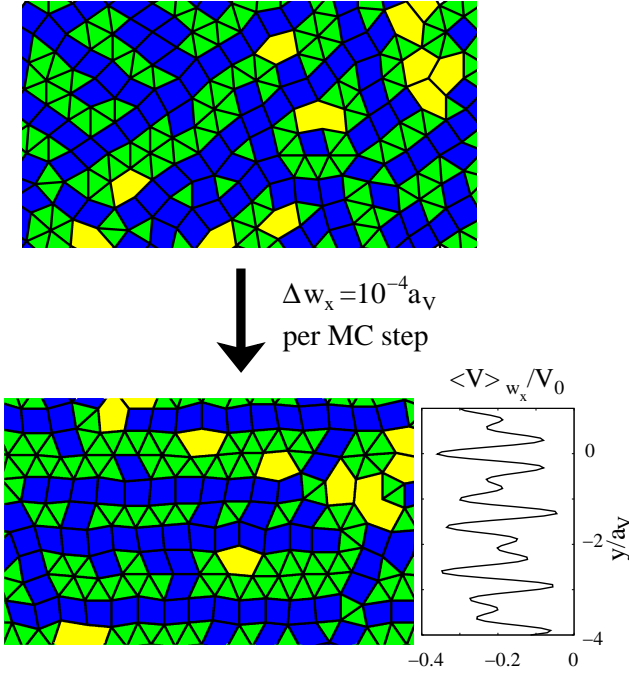$\Delta w_x = 10^{-4} a_V$
per MC step

$w_x/x = 0.15$

Fig. 11. Stabilization by a phasonic drift: Archimedean-like tiling phase (same parameters as in Fig. 10) obtained by Monte-Carlo simulations without phasonic displacement (top) and in a potential with a phasonic drift velocity of $\Delta w_x = 10^4 a_V$ per Monte-Carlo step (bottom). The small graph on the right-hand side shows the decagonal potential averaged over w_x as a function of y.

Fig. 12. Stabilization by a phasonic gradient: Archimedean-like tiling phase (same parameters as in Fig. 10) obtained by Monte-Carlo simulations without phasonic displacement (top) and in a potential with a phasonic gradient with $w_x/x = 0.15$ (bottom).

landscape such that existing potential wells disappear and reappear at other locations. Now consider a colloid in the decagonal laser field that experiences a sufficiently fast phasonic drift in w_x-direction, i.e., the relaxation time of the colloid within a potential well is much larger than the time scale on which the potential well vanishes due to the phasonic drift. Then one can introduce an effective potential $\langle V \rangle_{w_x}(y)$ for the colloids that is the decagonal potential $V(x,y)$ averaged over w_x. It is illustrated at the right hand side of Fig. 11. From Eq. (1) it is clear that $\langle V \rangle_{w_x}(y)$ does not depend on x or equals $V(x,y)$ averaged over the spatial coordinate x already introduced in Eq. (4), i.e.,

$$\langle V \rangle_{w_x}(y) = \langle V \rangle_x(y). \tag{9}$$

Clearly, such an effective potential can only support domains of Archimedean-like tilings oriented along the x-direction.

Another possibility of orienting domains of Archimedean-like tilings preferentially along the x-direction is to introduce a phasonic displacement field with a constant gradient in x-direction. Figure 13 shows the resulting decagonal interference pattern. The gradient in w_x destroys all continuous lines of low intensity in the potential landscape, except those in x-direction, as indicated by the red lines. Therefore, the Archimedean-like tiling is mainly oriented along the direction of the phasonic gradient, as illustrated in Fig. 12.
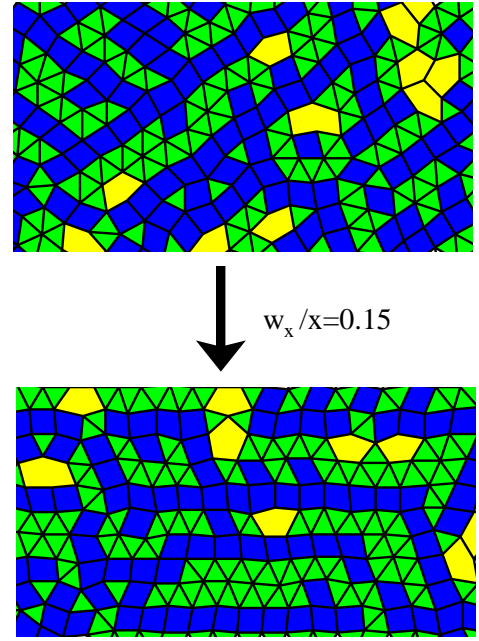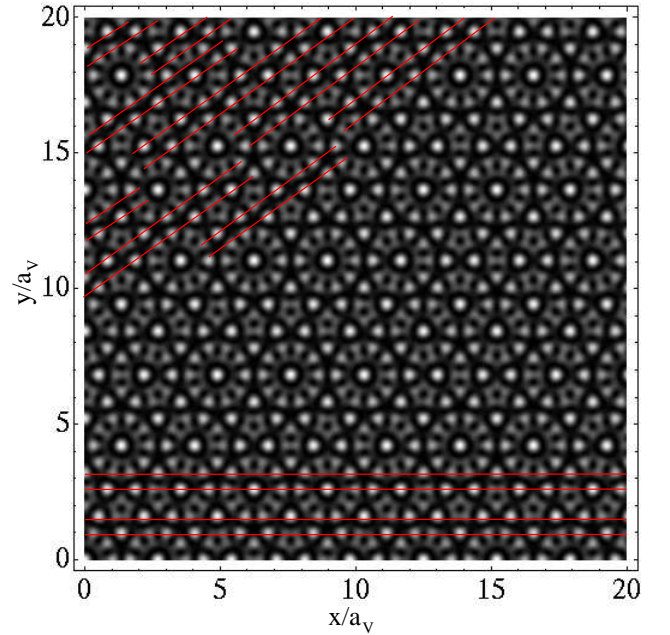

Fig. 13. Interference pattern of the decagonal laser field calculated from Eq. (1) when the phase ϕ_0 attached to wave vector $\mathbf{G}_0$ varies with a constant gradient, $\phi_0 = 0.2x/a_V$. Via Eq. (2) one can show that it creates a constant gradient in the x components of the phononic and phasonic displacements. As a result, the lines of low intensity are infinitly extended in x-direction whereas in all other directions they have a finite length (see, e.g., the dark stripes framed by the red lines). Similar jags are studied in [24, 25].

In the experimental interference pattern of Fig. 2c) some of the lines of low intensity just end in the middle of the pattern. This suggests that phasonic distortions are present, as we will now demonstrate. Suppose that the five laser beams in Fig. 2a) are not perfectly arranged around the vertical. For example, if the tilt angle θ_0 of beam 0 is larger than the other angles, the projected wave vector becomes $\mathbf{G}_0' = \mathbf{G}_0 + \Delta\mathbf{G}_0$ with $|\mathbf{G}_0'| > |\mathbf{G}_i|$ $(i = 0, 1...4)$. From Eq. (1) one finds that the deviation $\Delta\mathbf{G}_0$ can be interpreted as a constant gradient in the phase ϕ_0 attached to $\mathbf{G}_0$, $\phi_0 = \Delta\mathbf{G}_0 \cdot \mathbf{r}$. Using Eq. (2), this phase ϕ_0 can be decomposed into x components of the phononic and phasonic displacement fields with constant gradients. Therefore, laser beams that are not perfectly adjusted relative to the vertical lead to a substrate potential with phononic and phasonic distortions. Furthermore, such distortions can also be controlled intentionally by displacing one of the laser beams radially from its position on an ideal pentagon. This way one can create a preferred orientation for the Archimedean-like tiling, as discussed above.

In summary, phasonic drifts or distortions can be employed to grow large domains of an Archimedean-like tiling structure with a preferred orientation. These domains are stable when the phasonic drift is stopped or the phasonic distortion is removed.

6 Outlook and Conclusions

In this article we have studied the structure of Archimedean-like tiling phases that form in decagonal and tetradecagonal laser fields at certain densities. We have also demonstrated how the domain size of such tilings is influenced by phasonic distortions. In particular, if the interfering laser beams are not adjusted properly, phasonic displacement fields with a constant gradient arise. Interestingly, simulations using substrate potentials with further quasicrystalline symmetries also show similar phases. For example, in an interference pattern of eight beams we find rows of squares and triple or four-fold rows of triangles [Fig. 14(a)]. A laser field created by ten beams favors exactly the same structure as the decagonal potential obtained by five laser beams [Fig. 14(b)]. For the case of eleven beams, we also observe the characteristic rows of triangles and squares [Fig. 14(c)]. However, we are not able to analyze this ordering in more detail with respect to the order perpendicular to the rows, since the domains are too small. It is an interesting question for future research to understand, why such Archimedean-like tilings form at specific densities on substrates with different quasicrystalline symmetries. Depending on the specific rotational symmetry, all these structures consist of single and double (or even triple or four-fold) rows of triangles or squares that ultimately form a quasiperiodic order in one direction.

While on the decagonal substrate the rows in the Archimedean-like tiling form a Fibonacci chain, they show domains with periodic order on the tetradecagonal substrate interrupted by double rows of squares. We find that these double rows, as the double rows of triangles on the
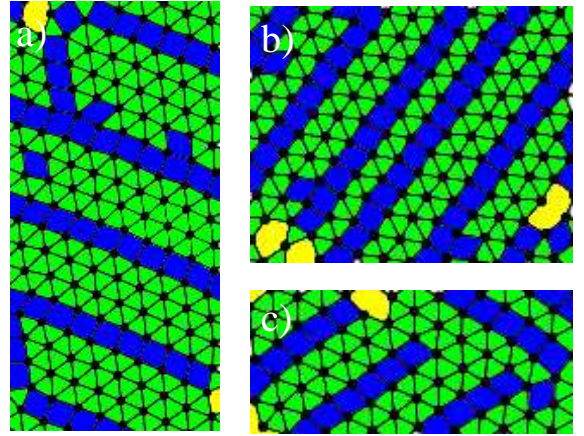

Fig. 14. Delaunay construction (as in Fig. 1) of simulation results that consist of rows of triangles and rows of squares in laser fields (of strength $V_0/(k_B T) = 50$) created by (a) eight beams ($a_S/a_V = 0.8$), (b) ten beams ($a_S/a_V = 0.7$), and (c) eleven beams ($a_S/a_V = 0.74$).

decagonal substrate, occur at symmetry centers of the substrate potential. As discussed in [20], the number of the symmetry centers is by a factor of 100 larger in the decagonal compared to the tetradecagonal substrate. Therefore, they enforce the formation of a Fibonacci chain in the first case, whereas in the tetradecagonal laser field larger periodic domains form due to the much smaller number of symmetry centers.

Amongst other phases (see Ref. [19]), Archimedean-like tilings appear as a compromise between structures favored either by the particle interaction or by the substrate potential. There is some evidence that they occur in experiments that study how atoms order on atomic surfaces with decagonal symmetry [18]. For the specific example of the Archimedean-like tiling, we have presented here Brownian dynamics simulations to demonstrate how the colloidal adsorbate reacts on phasonic distortions in the substrate. This rises the question if phasonic excitations are detectable in atomic substrates. The Archimedean-like tiling as an adsorbate phase might be a good candidate to visualize these excitations in the underlying substrate since resulting rearrangements in the rows of triangles and squares should be visible.

References

1. D. Shechtman, I. Blech, D. Gratias, and J. W. Cahn, Phys. Rev. Lett. **53**, 1951 (1984).
2. D. Levine and P.J. Steinhardt, Phys. Rev. Lett. **53**, 2477 (1984).
3. E. Macia, The role of aperiodic order in science and technology, Rep. Prog. Phys. **69**, 397 (2006).

4. R. McGrath, J. Ledieu, E. J. Cox, and R. D. Diehl, J. Phys.: Condens. Matter **14**, R119 (2002).
5. V. Fournée, T. C. Cai, A. R. Ross, T. A. Lograsso, J. W. Evans, and P. A. Thiel, Phys. Rev. B **67**, 033406 (2003).
6. M. Shimoda, T. J. Sato, A. P. Tsai, and J. Q. Guo, Phys. Rev. B **62**, 11288 (2000).
7. K. J. Franke, H. R. Sharma, W. Theis, P. Gille, Ph. Ebert, and K. H. Rieder, Phys. Rev. Lett. **89**, 156104 (2002).
8. J. Ledieu, J. T. Hoeft, D. E. Reid, J. A. Smerdon, R. D. Diehl, T. A. Lograsso, A. R. Ross, and R. McGrath, Phys. Rev. Lett. **92**, 135507 (2004).
9. R. A. Tasca, N. Ferralis, R. D. Diehl and M. W. Cole, J. Phys.: Condens. Matter **16**, S2911 (2004).
10. S. Curtarolo, W. Setyawan, N. Ferralis, R. D. Diehl, and M. W. Cole, Phys. Rev. Lett. **95**, 136104 (2005).
11. W. Setyawan, N. Ferralis, R. D. Diehl, M. W. Cole, and S. Curtarolo Phys. Rev. B **74**, 125425 (2006).
12. W. Setyawan, R. D. Diehl, N. Ferralis, M. W. Cole, and S. Curtarolo J. Phys.: Condens. Matter **19**, 016007 (2007).
13. B. Bilki, M. Erbudak, M. Mungan, and Y. Weisskopf, Phys. Rev. B **75**, 045437 (2007).
14. M. Mungan, Y. Weisskopf, and M. Erbudak, Phys. Rev. B **76**, 195443 (2007).
15. K. Pussi, M. Grierer, R.D. Diehl, J. Phys.: Condens. Matter **21**, 474213 (2009).
16. M. Schmiedeberg, J. Roth, and H. Stark, Phys. Rev. Lett. **97**, 158304 (2006).
17. M. Schmiedeberg, J. Roth, and H. Stark, Eur. Phys. J. E **24**, 367 (2007).
18. J. Mikhael, J. Roth, L. Helden, and C. Bechinger, Nature **454**, 501 (2008).
19. M. Schmiedeberg and H. Stark, Phys. Rev. Lett. **101**, 218302 (2008).
20. J. Mikhael, M. Schmiedeberg, S. Rausch, J. Roth, H. Stark, and C. Bechinger, submitted.
21. D. Levine, T.C. Lubensky, S. Ostlund, S. Ramaswamym, P.J. Steinhardt, and J. Toner, Phys. Rev. Lett. **54**, 1520 (1985).
22. J.E.S. Socolar, T.C. Lubensky, and P.J. Steinhardt, Phys. Rev. B **34**, 3345 (1986).
23. C.L. Henley, M. de Boissieu, and W. Steurer, Phil. Mag. **86**, 1131 (2006).
24. B. Freedman, R. Lifshitz, J.W. Fleischer, and M. Segev, Nature **440**, 1166 (2006).
25. B. Freedman, R. Lifshitz, J.W. Fleischer, and M. Segev, Nat. Mater. **6**, 776 (2007).
26. S.P. Gorkhali, J. Qi, and G.P. Crawford, J. Opt. Soc. Am. B **23**, 149 (2005).
27. B.V. Derjaguin and L. Landau, Acta Physicochimica (USSR) **14**, 633 (1941).
28. E.J. Verwey and J.T.G. Overbeek, *Theory of the Stability of Lyophobic Colloids* (Elsevier, Amsterdam, 1948).
29. W. Strepp, S. Sengupta, and P. Nielaba, Phys. Rev. E **66**, 056109 (2002).
30. N. Metropolis, A.W. Rosenbluth, M.N. Rosenbluth, A.H. Teller, and E. Teller, J. Chem. Phys. **21**, 1087 (1953).
31. B. Grünbaum and G.C. Shepard, *Tilings and Patterns* (W.H. Freeman, New York, 1987).
32. D.V. Talapin, E.V. Shevchenko, M.I. Bodnarchuk, X. Ye, J. Chen, and C.B. Murray, Nature **461**, 964 (2009).
33. A. Patrykiejew and S. Sokołowski, Phys. Rev. Lett. **99**, 156101 (2007).
34. M. Schmiedeberg and H. Stark, Phys. Rev. Lett. **100**, 019601 (2008).
35. A. Patrykiejew and S. Sokołowski, Phys. Rev. Lett. **100**, 019602 (2008).
36. W. Rzysko, A. Patrykiejew and S. Sokołowski, J. Phys. Cond. Mat. **20**, 494226 (2008).